# Flux Invariants for Shape

Pavel Dimitrov[†]          James N. Damon[§]          Kaleem Siddiqi[†]

[†]School of Computer Science
McGill University
Montreal, Canada

[§]Department of Mathematics
University of North Carolina, Chapel Hill
Chapel Hill, North Carolina, USA

## Abstract

*We consider the average outward flux through a Jordan curve of the gradient vector field of the Euclidean distance function to the boundary of a 2D shape. Using an alternate form of the divergence theorem, we show that in the limit as the area of the region enclosed by such a curve shrinks to zero, this measure has very different behaviours at medial points than at non-medial ones, providing a theoretical justification for its use in the Hamilton-Jacobi skeletonization algorithm of [7]. We then specialize to the case of shrinking circular neighborhoods and show that the average outward flux measure also reveals the object angle at skeletal points. Hence, formulae for obtaining the boundary curves, their curvatures, and other geometric quantities of interest, can be written in terms of the average outward flux limit values at skeletal points. Thus this measure can be viewed as a Euclidean invariant for shape description: it can be used to both detect the skeleton from the Euclidean distance function, as well as to explicitly reconstruct the boundary from it. We illustrate our results with several numerical simulations.*

## 1. Introduction

In recent years there has been a resurgence of interest in representations based on the Blum skeleton, and extensions to 3D, for shape representation and analysis have been developed [9, 5, 8]. A number of abstractions related to the skeleton have been proposed, and algorithms for a diverse range of computer vision and medical imaging applications have been developed. These include shape segmentation, shape matching, view-based object recognition and indexing. Although the possibility of using the Blum skeleton in such domains has long been considered, only recently have robust and efficient algorithms for computing such representations been developed. This paper focuses on one class of such algorithms, those which utilize the average outward flux of the gradient vector field of the signed Euclidean dis-tance function [7, 3, 6].

This paper makes several contributions. First, an alternate form of the divergence theorem is introduced in order to investigate the behaviour of the gradient vector field of the Euclidean distance function at medial points, where it is discontinuous. Second, we show that the limiting behaviour of the average outward flux of this vector field through a Jordan curve as the area it encloses shrinks to zero, is very different at medial points than at non-medial ones, providing a strong theoretical justification for its use in the Hamilton-Jacobi skeletonization algorithm [7]. Third, we specialize to the case of shrinking circular neighborhoods and show that the average outward flux measure also reveals the object angle at each of the three types of skeletal points: 1) regular points, 2) branch points and 3) end- points. Hence, formulae for obtaining the boundary curves, their curvatures, and other geometric quantities of interest, can be written in terms of the average outward flux limit values at skeletal points. We illustrate our results with several numerical simulations.

## 2. Flux and Divergence

### 2.1. Preliminaries

We shall consider a *shape* to be any path connected space $X$ in the plane, for which the boundary $\partial X$ is given by $C^3$ curves. For each point $P \in \mathbb{R}^2$ in the plane we define a distance function $D : \mathbb{R}^2 \to \mathbb{R}$

$$D(P) = \inf_{Q \in \partial X} d(P, Q)$$

where $d(P, Q)$ is the Euclidean distance between $P$ and $Q$. Given our assumptions on $X$, $D$ is a continuously differentiable function everywhere except on the skeleton.

Now, for each point $P \in \mathbb{R}^2$, define the set $P_C = \{(x, y) \in \partial X \mid D(x, y) = D(P)\}$. Thus, $P_C$ contains all points on the boundary that are closest to $P$. The *skeleton* of a shape $X$, denoted $S(X)$, is the set of points for which

there are two or more closest boundary points

$$S(X) = \{P \in X \mid |P_C| \ge 2\}.$$

Technically, this excludes end-points of the skeleton since an end-point coincides with the center of curvature of a boundary point $Q \in \partial X$ that is a local maximum of positive curvature.

The distance function gradient vector field $\dot{\mathbf{q}} = \nabla D$, is continuous and has magnitude one, except at skeletal points where it is not continuous. Hence, with the exception of skeletal points, $\nabla D$ can be parametrized by its orientation at each point in the plane. With $\theta(x, y) : \mathbb{R}^2 \to [0, 2\pi]$ being the orientation of the gradient vector at $(x, y)$ and $R(\theta)$ being the rotation matrix with argument $\theta$, we have $\nabla D(x, y) = R(\theta(x, y))\mathbf{e}_1$, where $\mathbf{e}_1 = (1, 0)$, and $\nabla D(x, y) \cdot \mathbf{v} = \cos(\alpha - \theta(x, y))$, where $\mathbf{v}$ is any unit vector with orientation $\alpha$.

We now define the outward flux and the average outward flux of the gradient vector field $\dot{\mathbf{q}}$ through a Jordan curve. Let $\mathcal{N}$ be the *outward* normal at each point on the boundary $\partial R$ of such a curve, and $\mathrm{d}s$ be an arc-length element.

**Definition 1** *The outward flux of $\dot{\mathbf{q}}$ through $\partial R$ is given by*

$$\int_{\partial R} \langle\, \dot{\mathbf{q}}, \mathcal{N}\, \rangle \ \mathrm{d}s.$$

**Definition 2** *The average outward flux of $\dot{\mathbf{q}}$ through $\partial R$ is given by*

$$\frac{\int_{\partial R} \langle\, \dot{\mathbf{q}}, \mathcal{N}\, \rangle \ \mathrm{d}s.}{\int_{\partial R} \ \mathrm{d}s.}$$

## 2.2. An Extension of the Divergence Theorem

If $\dot{\mathbf{q}}$ is differentiable over a region $R$ with boundary $\partial R$, the standard form of the divergence theorem states that

$$\int_{R} \mathrm{div}(\dot{\mathbf{q}}) \ \mathrm{d}v \equiv \int_{\partial R} \langle\, \dot{\mathbf{q}}, \mathcal{N}\, \rangle \ \mathrm{d}s. \qquad (1)$$

Here $\mathrm{d}v$ is an area element. In other words, the integral of the divergence of the vector field over a region is given by the outward flux of the vector field through that region's bounding contour. We shall now develop an extension of the divergence theorem which can be applied to investigate properties of the vector field $\dot{\mathbf{q}} = \nabla D$ at skeletal points, where it is discontinuous. Figure 1 illustrates the set up for the calculation which follows.

Let $S$ be a branch of the skeleton and let $R = R_1 \cup R_2$ be a path connected region which intersects it. Let $\partial R = C_1 \cup C_2$ and $C_3 = S \cap R$. Let $C_{3t}^{'}, C_{3t}^{''}$ be parallel curves to $C_3$ which approach $C_3$ as $t \to 0$. Let $R_{1t}$ and $R_{2t}$ be the regions obtained from $R_1$ and $R_2$ by removing the region between the curves $C_{3t}^{'}$ and $C_{3t}^{''}$ Finally, let $\dot{\mathbf{q}}_+$ denote $\dot{\mathbf{q}}$ above $S$ and $\dot{\mathbf{q}}_-$ denote $\dot{\mathbf{q}}$ below $S$.
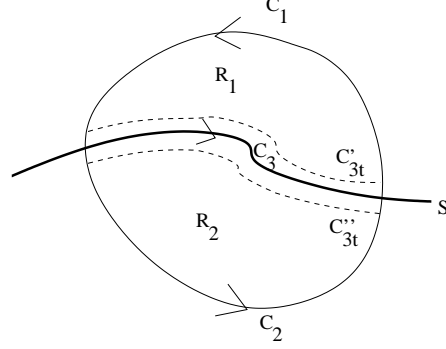


**Figure 1**. A region $R$ which intersects a branch of the skeleton $S$.

The outward flux of $\dot{\mathbf{q}}$ through $\partial R$ is given by

$$\int_{\partial R} \langle\, \dot{\mathbf{q}}, \mathcal{N}\, \rangle \ \mathrm{d}s = \int_{C_1} \langle\, \dot{\mathbf{q}}, \mathcal{N}\, \rangle \ \mathrm{d}s + \int_{C_2} \langle\, \dot{\mathbf{q}}, \mathcal{N}\, \rangle \ \mathrm{d}s.$$

Applying the divergence theorem to $R_{1t}$ and $R_{2t}$

$$\int_{R_{1t}} \mathrm{div}(\dot{\mathbf{q}}) \ \mathrm{d}v = \int_{C_{1t}} \langle\, \dot{\mathbf{q}}, \mathcal{N}\, \rangle \ \mathrm{d}s + \int_{C_{3t}^{'}} \langle\, \dot{\mathbf{q}}, \mathcal{N}\, \rangle \ \mathrm{d}s,$$

$$\int_{R_{2t}} \mathrm{div}(\dot{\mathbf{q}}) \ \mathrm{d}v = \int_{C_{2t}} \langle\, \dot{\mathbf{q}}, \mathcal{N}\, \rangle \ \mathrm{d}s + \int_{-C_{3t}^{''}} \langle\, \dot{\mathbf{q}}, \mathcal{N}\, \rangle \ \mathrm{d}s.$$

Adding the above two equations we have

$$\int_{R_{1t}} \mathrm{div}(\dot{\mathbf{q}}) \ \mathrm{d}v + \int_{R_{2t}} \mathrm{div}(\dot{\mathbf{q}}) \ \mathrm{d}v =$$

$$\int_{C_{1t}} \langle\, \dot{\mathbf{q}}, \mathcal{N}\, \rangle \ \mathrm{d}s + \int_{C_{2t}} \langle\, \dot{\mathbf{q}}, \mathcal{N}\, \rangle \ \mathrm{d}s +$$

$$\int_{C_{3t}^{'}} \langle\, \dot{\mathbf{q}}, \mathcal{N}\, \rangle \ \mathrm{d}s + \int_{-C_{3t}^{''}} \langle\, \dot{\mathbf{q}}, \mathcal{N}\, \rangle \ \mathrm{d}s.$$

It is a standard property that the tangent to the skeleton bisects the the angle between $\dot{\mathbf{q}}_+$ and $\dot{\mathbf{q}}_-$ at a skeletal point (see Figure 2). Thus, on $C_3$ we have

$$\langle\, \dot{\mathbf{q}}_+, \mathcal{N}_+\, \rangle = \langle\, \dot{\mathbf{q}}_-, \mathcal{N}_-\, \rangle, \qquad (2)$$

where $\mathcal{N}_+, \mathcal{N}_-$ denote the normals to $C_3$ from above and from below, respectively. Thus, one can take the limit as $t \to 0$ of both sides of the above equation to obtain the following extension of the divergence theorem

**Theorem 1** *For a path connected region $R$ which contains part of a skeletal curve $S$, the divergence of the vector field $\dot{\mathbf{q}}$ is related to its flux through $\partial R$ by the following equation*

$$\int_{R = R_1 \cup R_2} \mathrm{div}(\dot{\mathbf{q}}) \ \mathrm{d}v =$$

$$\int_{\partial R} \langle\, \dot{\mathbf{q}}, \mathcal{N}\, \rangle \ \mathrm{d}s + 2 \int_{C_3} \langle\, \dot{\mathbf{q}}, \mathcal{N}_{C_3}\, \rangle \ \mathrm{d}s.$$

Although the divergence theorem fails for such regions because $\dot{\mathbf{q}}$ is discontinuous on $C_3$, the last integral is well defined due to Eq. 2; we either take $\dot{\mathbf{q}} = \dot{\mathbf{q}}_+$ and $\mathcal{N}_{C_3} = \mathcal{N}_+$ or $\dot{\mathbf{q}} = \dot{\mathbf{q}}_-$ and $\mathcal{N}_{C_3} = \mathcal{N}_-$. Because $\langle\, \dot{\mathbf{q}}, \mathcal{N}_{C_3}\, \rangle$ is in the interval $(0, 1]$ on the skeleton, it also follows that

$$\int_{\partial R} \langle\, \dot{\mathbf{q}}, \mathcal{N}\, \rangle \; \mathrm{d}s \geq \int_R \mathrm{div}(\dot{\mathbf{q}}) \; \mathrm{d}v - 2 \times length(C_3).$$

## 2.3. Intrinsic Meaning of the Outward Flux

It is a standard fact that the quantity $\int_R \mathrm{div}(\dot{\mathbf{q}}) \; \mathrm{d}v$, and hence the outward flux of $\dot{\mathbf{q}}$ through $\partial R$, measures the degree to which the flow produced by the vector field $\dot{\mathbf{q}}$ is *area preserving* in 2D (or volume preserving in 3D). This can be seen by applying the transport theorem [1] (p. 10) to the area enclosed by $\partial R$. This quantity is highly non-intrinsic in that it is strongly dependent on $\partial R$, and is zero only for very special cases, those where the vector field $\dot{\mathbf{q}}$ is locally parallel. Thus, calculations such as those reported in [10], where the outward flux measure introduced in [6] is related to a notion of Blum's ligature, do not hold in the general case. This also raises the question of how such a measure could be used to distinguish skeletal points from non-skeletal ones, as suggested in [6, 3]. The answer, as we will now see, is to consider the limiting behavior of the average outward flux of $\dot{\mathbf{q}} = \nabla D$, as the region enclosed shrinks to zero. This measure is at the heart of the Hamilton-Jacobi skeletonization algorithm in [7].

## 2.4. Limiting Behaviour

We now consider the limit values of the outward flux and the average outward flux, of the vector field $\dot{\mathbf{q}} = \nabla D$ through a convex curve that is the boundary $\partial R$ of a region $R$, as the region shrinks to a point. The results reported here are actually a special case of a more general result which applies to the case of any shrinking convex domain, and which extends to higher dimensions [2].

We begin by considering the case where the limit point $P$ does not lie on the skeleton and hence Eq. (1) applies. We can write

$$\int_R \mathrm{div}(\dot{\mathbf{q}}) \; \mathrm{d}v \equiv \int_0^L \langle\, \dot{\mathbf{q}_P} + \delta(s), \mathcal{N}\, \rangle \; \mathrm{d}s$$

where $L$ is the Euclidean length of $\partial R$, $\dot{\mathbf{q}_P}$ is the value of the vector field at the limit point $P$ and $\delta(s)$ is the quantity added to get the value of $\dot{\mathbf{q}}$ at neighboring points on $\partial R$ ($\dot{\mathbf{q}}$ is continuous at $P$). In the limit as $L \to 0$ we have

$$\lim_{L\to 0} \left( \int_0^L \langle\, \dot{\mathbf{q}_P}, \mathcal{N}\, \rangle \; \mathrm{d}s + \int_0^L \langle\, \delta(s), \mathcal{N}\, \rangle \; \mathrm{d}s \right).$$

It is easy to see that the second integral goes to zero due to the fact that $\delta(s)$ goes to zero. The first integral also goes to

zero due to the fact that $\partial R$ is a closed curve. Thus, the limit value obtained for the outward flux value at a non-skeletal point is zero. By essentially the same argument, the limit value obtained for the average outward flux value at such a point is also zero.

We now consider the second case where the limit point is a skeletal point and hence Theorem 1 applies, which we rewrite as

$$\int_{\partial R} \langle\, \dot{\mathbf{q}}, \mathcal{N}\, \rangle \; \mathrm{d}s = \int_R \mathrm{div}(\dot{\mathbf{q}}) \; \mathrm{d}v - 2\int_{C_3} \langle\, \dot{\mathbf{q}}, \mathcal{N}_{C_3}\, \rangle \; \mathrm{d}s.$$

By the same argument presented for the first case above, the first integral on the right hand side goes to zero in the limit as $R \to 0$. The second integral on the right hand side can be written as

$$-2\int_{C_3} \langle\, \dot{\mathbf{q}_P} + \delta(s), \mathcal{N}_{C_3}\, \rangle \; \mathrm{d}s$$

where $P$ is the limit point and $\delta(s)$ is the quantity added to get the value of $\dot{\mathbf{q}}$ at neighboring points on $C_3$. Owing to the fact that the integrand is in $(0, 1]$ (a special property of skeletal points), the value of this second integral is bounded above by $-2 \times (\inf_{C_3} \langle\, \dot{\mathbf{q}}_{C_3}, \mathcal{N}_{C_3}\, \rangle) \times length(C_3)$ and below by $-2 \times length(C_3)$. Thus we deduce that the limit value of the outward flux at a skeletal point is also zero, due to the multiplicative length term. On the other hand, when the average outward flux is considered (see Definition 2), the limit value reached as the region shrinks to a skeletal point $P$ is $-2 \langle\, \dot{\mathbf{q}_P}, \mathcal{N}_P\, \rangle$.

Summarizing the above results, we have the property that whereas the limit value of the outward flux is zero for both skeletal and non-skeletal points, the average outward flux has a different limiting behaviours at skeletal points than at non-skeletal ones, providing a theoretical justification for its use in the Hamilton-Jacobi skeletonization algorithm [7].

# 3. Circular Neighborhoods

We now specialize the average outward flux calculation to the case of circular neighborhoods shrinking to a skeletal point. We shall treat the three cases of regular points, branch points and end-points of the skeleton separately.

## 3.1. Regular Skeletal Points

A *regular skeletal point* $P$ is one for which $P_C = \{Q_1, Q_2\}$ for $Q_1 \neq Q_2$. Let $\mathbf{n}_1$ and $\mathbf{n}_2$ be the unit inward normals to the boundary at $Q_1$ and $Q_2$ respectively. Let $\mathbf{t}_P$ be the unit tangent vector to the skeleton at $P$ and define the *object angle* at $P$ to be $\alpha(P) \in [0, \pi/2]$, such that

$$\mathbf{n}_1 \cdot \mathbf{n}_2 = \cos 2\alpha(P).$$

It follows that $\mathbf{n}_i \cdot \mathbf{t}_P = \cos \alpha(P)$ for $i = 1, 2$ (see Figure 2).
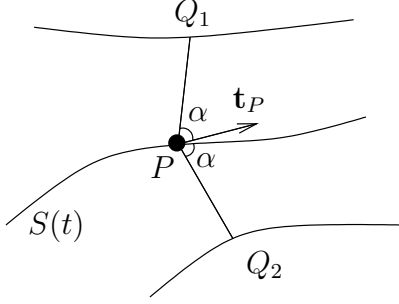
**Figure 2**. The object angle $\alpha = \alpha(P)$ at a simple skeletal point $P$. Here $S(t)$ is a parameterization of the skeleton curve. Hence, $\mathbf{t}_P = S'(t_0)$ is the tangent at $t_0$, i.e. where $P = S(t_0)$.
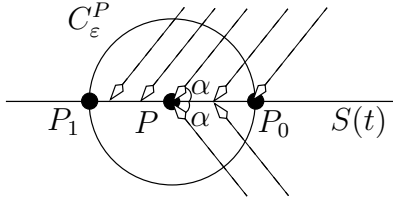


**Figure 3**. The distance function gradient vector field in the $\varepsilon$-neighborhood of $P$ is given by a step function – one value for the "top" semi-circle and another for the "bottom" one. Both these vectors form an angle of $\alpha = \alpha(P)$ with $\mathbf{t}_P$, since the skeleton is assumed to cut $C_\varepsilon^P$ in half at $P_0$ and $P_1$.

Now, let $C_\varepsilon^P$ be the circle with radius $\varepsilon$ centered at $P$. Let $C_\varepsilon^P : [0, 2\pi] \to \mathbb{R}^2$ be given by

$$C_\varepsilon^P(s) = \varepsilon(\cos(s + \theta(\mathbf{t}_P)), \sin(s + \theta(\mathbf{t}_P)) + P, \quad (3)$$

where $C_\varepsilon^P(0) = P + \varepsilon\mathbf{t}_P$ and $C_\varepsilon^P(\pi) = P - \varepsilon\mathbf{t}_P$. Now consider Figure 3. Here, it is assumed that the gradient field has one value along $C_\varepsilon^P(s)$ for $s \in (0, \pi)$ and another for $s \in (\pi, 2\pi)$. Also, both $C_\varepsilon^P(0) = P_0$ and $C_\varepsilon^P(\pi) = P_1$ are on the skeleton. Let the outward normal of this circle at $s$ be $\mathcal{N}(s)$. Hence, the outward flux of $\nabla D$ though $C_\varepsilon^P(s)$ is

$$\mathcal{F}_\varepsilon(P) = \int_0^{2\pi\varepsilon} \big\langle \nabla D(C_\varepsilon^P(s)), \mathcal{N}(s) \big\rangle \, \mathrm{d}s$$

$$= -\varepsilon \int_0^\pi \cos(\alpha - s) \, \mathrm{d}s - \varepsilon \int_\pi^{2\pi} \cos(-\alpha - s) \, \mathrm{d}s$$

$$= -4\varepsilon \sin(\alpha)$$

Notice that this calculation holds regardless of the orientation of $\mathbf{t}_P$. However, it makes very strict assumptions that do not hold in most situations. Fortunately, the general case is similar to this one.

There are only two differences: (1) $C_\varepsilon^P(0)$ and $C_\varepsilon^P(\pi)$ may not be on the skeleton, and (2) the distance function gradient field may take on more than two values along $C_\varepsilon^P(s)$ for $s \in [0, 2\pi]$. For small enough $\varepsilon$, the circle will intersect the skeleton at precisely two points, which we label $P_0 = C_\varepsilon^P(\delta_0)$ and $P_1 = C_\varepsilon^P(\pi + \delta_1)$. Thus, the distance function gradient field is continuous on $C_\varepsilon^P(s)$ for $s \in I_0 = (\delta_0, \pi+\delta_1)$ and also for $s \in I_1 = (\pi+\delta_1, 2\pi-\delta_0)$ [1]. However, it may take on more than one value in the intervals $I_0$ and $I_1$. Define $\beta_0(s)$ and $\beta_1(s)$ on $I_0$ and $I_1$ respectively, to account for such eventualities:

$$\mathbf{t}_P \cdot \theta(C_\varepsilon^P(s)) = \cos\left(\alpha(P) + \beta_0(s)\right) \quad, \; s \in I_0$$

$$\mathbf{t}_P \cdot \theta(C_\varepsilon^P(s)) = \cos\left(-\alpha(P) + \beta_1(s)\right), \; s \in I_1.$$

Therefore, the outward flux calculation for regular skeletal points becomes

$$\begin{aligned}
\mathcal{F}_\varepsilon(P) &= \int_0^{2\pi\varepsilon} \big\langle \nabla D(C_\varepsilon^P(s)), \mathcal{N}(s) \big\rangle \, \mathrm{d}s \\
&= -\varepsilon \int_{\delta_0}^{\pi+\delta_1} \cos(\alpha + \beta_0(s) - s) \, \mathrm{d}s \\
&\quad -\varepsilon \int_{\pi+\delta_1}^{2\pi-\delta_0} \cos(-\alpha + \beta_1(s) - s) \, \mathrm{d}s.
\end{aligned}$$

The continuity of the distance function gradient field along the circle implies that both $\beta_0(s)$ and $\beta_1(s)$ are continuous functions. Further, as $\varepsilon \to 0$, necessarily

$$\lim_{\varepsilon \to 0} \sup_{s \in [\delta_0, \pi+\delta_1]} |\beta_0(s)| = 0$$

$$\lim_{\varepsilon \to 0} \sup_{s \in [\pi+\delta_1, 2\pi-\delta_0]} |\beta_1(s)| = 0.$$

Also, since the skeletal curve has continuous tangents, we must have that $\lim_{\varepsilon \to 0} \delta_i = 0$ for $i = 0, 1$. Therefore the average outward flux through a shrinking circular region is given by

$$\lim_{\varepsilon \to 0} \frac{\mathcal{F}_\varepsilon(P)}{2\pi\varepsilon} = -\frac{2}{\pi} \sin \alpha.$$

### 3.2. Skeletal End-Points

Let $P$ be a skeletal end-point. Let the point $Q_\varepsilon$ be on the branch which is at distance $\varepsilon$ from $P$. Choose $\varepsilon$ small enough so that $Q_\varepsilon$ is a regular skeletal point. Thus, the object angle is well defined for $Q_\varepsilon$. Now, let

$$\alpha_P = \lim_{\varepsilon \to 0} \alpha(Q_\varepsilon).$$

This limit makes sense, because the circle[2] $C_\varepsilon^P$ intersects the skeleton at a single point. Also, the object angle varies continuously along a skeletal branch.

---

[1] However, it is not necessarily continuous on the closure of $I_0 \cup I_1$.
[2] Here $C_\varepsilon^P$ is as defined in Eq. (3) but $\mathbf{t}_P = \lim_{\varepsilon \to 0} \mathbf{t}_{Q_\varepsilon}$.
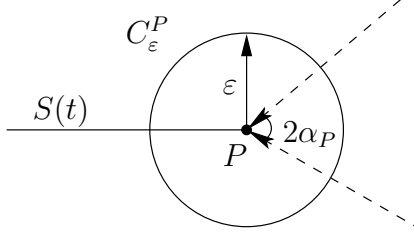
**Figure 4**. A circular neighborhood of radius $\varepsilon$ around the end-point $P$. Along the arc of angle $2\alpha_P$ the gradient vectors agree (in orientation) with the normals to $C_\varepsilon^P$. Along the arc "above" $S(t)$ the gradient vectors all form an angle of $\alpha_P$ with $S'(0) = \mathbf{t}_P$. Similarly, for the arc "below," this angle is $-\alpha_P$.

Now consider Figure 4. Along the arc $arc_{\alpha_P}$ opposite to the skeleton curve, the distance function gradient field must coincide with the inner normals of the circle. This is because the end-point results from the collapse of a circular arc (possibly a point if $\alpha_P = 0$) on the boundary. On the rest of the circle, the distance function gradient field behaves as if $P$ were a regular skeletal point. Thus,

$$\mathcal{F}_\varepsilon(P) = - \varepsilon \int_{-\alpha_P}^{\alpha_P} \mathrm{d}s$$

$$- \varepsilon \int_{\alpha_P\varepsilon}^{\pi+\delta} \cos(\alpha_P + \beta_0(s) - s)\, \mathrm{d}s$$

$$- \varepsilon \int_{\pi+\delta}^{2\pi-\alpha_P} \cos(-\alpha_P + \beta_1(s) - s)\, \mathrm{d}s$$

where $\delta$ and $\beta_i(s)$ account for the circle not intersecting the skeleton midway and the distance function gradient field not being strictly a step function on $C_\varepsilon^P - arc_{\alpha_P}$. Therefore,

$$\lim_{\varepsilon \to 0} \frac{\mathcal{F}_\varepsilon(P)}{2\pi\varepsilon} = -\tfrac{1}{\pi}(\alpha_P + \sin\alpha_P)$$

since, as $\varepsilon \to 0$, $\delta$, $\beta_0(s)$ and $\beta_1(s)$ vanish. Notice, however, that $\alpha_P = 0$ if the end-point is generated from a contour segment where the curvature is continuous.

### 3.3. Skeletal Junction Points

Let $P$ be a skeletal junction point; that is where $n$ skeletal curves meet. Let these curves be given by parameterizations $S_i(t)$ so that $S_i(0) = P$. Consider a circle of radius $\varepsilon$ centered at $P$. Denote it $C_\varepsilon^P$. For small enough $\varepsilon$, $C_\varepsilon^P$ intersects the skeleton at precisely $n$ regular points. Refer to them as $Q_\varepsilon^i = S_i(\varepsilon)$. Hence, to each there is a corresponding object angle. Define $\alpha_i$ as

$$\alpha_i = \lim_{\varepsilon \to 0} \alpha_{Q_\varepsilon^i}.$$
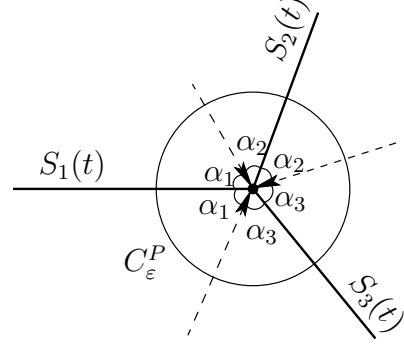


**Figure 5**. A circular neighborhood of radius $\varepsilon$ around the junction point $P$. There are three skeletal curves denoted by $S_1(t)$, $S_2(t)$ and $S_3(t)$ respectively. The dashed lines link $P$ and its closest points on the boundary (i.e. points in $P_C$). Note that $\alpha_1 + \alpha_2 + \alpha_3 = \pi$.

Now consider Figure 5. It suggests that $\sum_i 2\alpha_i = 2\pi$. Indeed, $\alpha_i$ is the angle between $S_i'(0)$ [3] and the line joining $P$ to some point in $P_C$. To compute the outward flux through $C_\varepsilon^P$, we can divide the circle into $n$ arcs, each corresponding to a skeletal curve. In particular, for $S_i(t)$ this would be the arc of angle $2\alpha_i$. For example, in Figure 5, the arc corresponding to $S_1(t)$ is the union of the two arcs of angle $\alpha_1$. Notice that the distance function gradient field along that arc behaves like that of a regular skeletal point with object angle $\alpha_i$. Hence, the outward flux through it is

$$\mathcal{F}_\varepsilon(arc_i) = - \varepsilon \int_{\delta_i}^{\alpha_i} \cos(\alpha_i + \beta_{0,i}(s) - s)\, \mathrm{d}s$$

$$- \varepsilon \int_{-\alpha_i}^{\delta_i} \cos(-\alpha_i + \beta_{1,i}(s) - s)\, \mathrm{d}s$$

where $\delta_i$, $\beta_{0,i}(s)$ and $\beta_{0,i}(s)$ all vanish as $\varepsilon \to 0$. Thus, the total outward flux is $\mathcal{F}_\varepsilon(P) = \sum_{i=1}^{n} \mathcal{F}_\varepsilon(arc_i)$ and the average outward flux becomes

$$\lim_{\varepsilon \to 0} \frac{\mathcal{F}_\varepsilon(P)}{2\pi\varepsilon} = -\frac{1}{\pi} \sum_{i=1}^{n} \sin\alpha_i.$$

### 3.4. Non-Skeletal Points

Now, let $P$ be a non-skeletal point. In particular, there exists an $\varepsilon$ small enough, so that $C_\varepsilon^P$ contains no skeletal points. Hence, the distance function gradient field along the circle is continuous. Thus, we can write

$$\mathcal{F}_\varepsilon(P) = \varepsilon \int_0^{2\pi} \cos(\alpha + \beta(s) - s)\, \mathrm{d}s,$$

---

[3] Here $S_i'(0) = \lim_{t \to 0_+} S_i'(t)$.

| Point Type | $\lim_{\varepsilon \to 0} \dfrac{\mathcal{F}_\varepsilon(P)}{2\pi\varepsilon}$ |
|---|---|
| Regular Points (Figure 2) | $-\frac{2}{\pi}\sin\alpha$ |
| End-Points (Figure 4) | $-\frac{1}{\pi}(\sin\alpha - \alpha)$ |
| Junction Points (Figure 5) | $-\frac{1}{\pi}\sum_{i=1}^{n}\sin\alpha_i$ |
| Non-Skeletal Points | $0$ |

**Table 1**. A summary of results relating the limit values of the average outward flux to the object angle for shrinking circular neighborhoods. Note that for contours of type $C^3$, $\alpha$ will be zero for the case of end-points.

where $\lim_{\varepsilon \to 0} \sup_{s \in [0, 2\pi]} |\beta(s)| = 0$. Hence,

$$\lim_{\varepsilon \to 0} \frac{\mathcal{F}_\varepsilon(P)}{2\pi\varepsilon} = \frac{1}{2\pi}\int_0^{2\pi} \cos(\alpha - s)\, \mathrm{d}s = 0.$$

### 3.5. Boundary Reconstruction

These results also suggest a method for parameterizing the boundary curves given a parameterization of the skeletal curves. Let $S(t)$ be an arc-length parameterization of a skeletal curve and denote by $\alpha(t)$ and $r(t)$ the object angle at $S(t)$ and distance to boundary, respectively (see Figure 2; if $S(t) = P$ then $r(t) = d(P, Q_1) = d(P, Q_2)$). Note that the object angle can in turn be written in terms of the average outward flux limit values, as summarized in Table 1. Assume that $r(t)$ is monotonically decreasing, i.e., segment the skeletal curve if necessary, The two boundary curves that created this skeleton curve are given by

$$C_{1,2}(t) = S(t) + r(t)R(\pm\alpha(t))S'(t), \qquad (4)$$

where $S'(t)$ is the tangent to the skeleton at $S(t)$ and $R(\alpha)$ denotes the rotation of $S'(t)$ by $\alpha$.

### 4. Experimental Results

We have performed a several numerical simulations to corroborate findings as well as to demonstrate the applicability of our results. Figure 6 presents an overview of the steps involved in the experiments. We begin with a binary image and trace its discrete boundary to get an ordered list of pixels connected with line segments. Thus, a closed curve $C(t) : \mathbb{R} \to \mathbb{R}^2$ is obtained[4] (step 1). It is now possible to define a Euclidean distance function $D : \mathbb{R}^2 \to \mathbb{R}$ on the whole plane. In this particular setting, $D(x, y)$ can be computed exactly by considering all line segments and returning the distance to the segment closest to a point $(x, y)$. Thus, it is also possible to approximate the average outward flux of $\nabla D$ through a circle of radius $\varepsilon > 0$ centered anywhere in $\mathbb{R}^2$. Furthermore, the precision of the computation depends only on the hardware. Hence, the results summarized in Table 1 can be used to obtain the skeleton of the curve. The exact method is described in [3]. This algorithm returns a discrete sampling of the skeletal curves as sequences of points (step 2). Thus, tangents at skeletal points may be approximated. The radius function is available through $D(x, y)$, and the object angle $\alpha$ can be obtained from the flux at regular points. This information can then be used to reconstruct boundary sections corresponding to regular skeletal points (step 3), see Section 3.5.

Figure 7 provides additional examples of the above computation. Figure 8 compares the accuracy of the method to that of an exact calculation. The profile on the left uses straight lines to show the association of regular skeletal points with their bi-tangent points on the contour (the black circles). Here the association has been determined by using the average outward flux limit values to obtain the object angle. The profile on the right demonstrates an exact computation, where the bi-tangent points are obtained by connecting each regular skeletal point to its two closest contour points. Notice how similar the two computations are. In fact, the average outward flux calculation can be performed with arbitrary precision[5]. It should be pointed out that certain portions of the contour have not been reconstructed because the end-points of the skeleton have been chosen to satisfy an object angle threshold (above $30°$). Consequently, the end-points shown, although very close to the real ones [6], may not be actual end-points of the skeleton. Thus, to approximate the missing portions of the contour, it would be necessary to draw the circular arcs corresponding to the approximate end-points.

### 5. Conclusion

We have derived an alternate form of the divergence theorem that accounts for singularities in the gradient vector field of the Euclidean distance function to the boundary of a shape and have used it to establish a criterion for detect-

---

[4]The pixel locations are smoothed to account for jaggedness inherent in all discrete images.

[5]Given a sub-sampling of a skeletal curve, it can be improved by numerical methods. One can use the fact that a skeletal point is a maximum along the gradient line leading to it. Thus, the Nelder-Mead Simplex method in 1D (see [4]) may be applied to precisely interpolate new points.

[6]In fact it can be shown that over 90% of the area due to protrusions is kept, although a detailed analysis is beyond the scope of this paper.
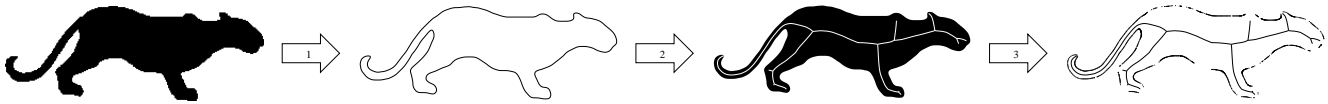
**Figure 6**. (1) From a binary image, the boundary is extracted and represented as a continuous curve. (2) The skeleton is computed. (3) Using the average outward flux and radius values along the skeleton, the boundary is reconstructed.
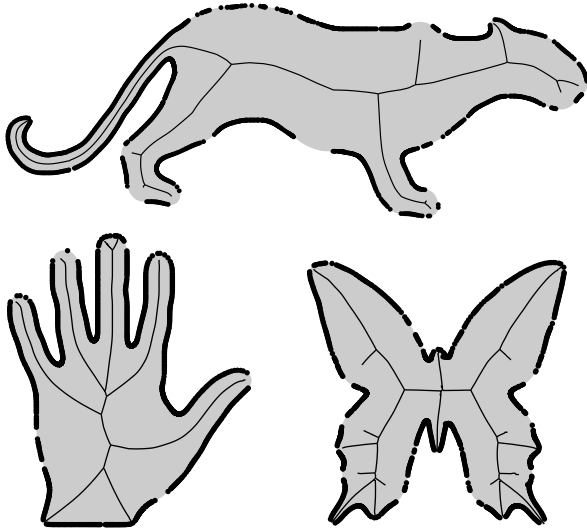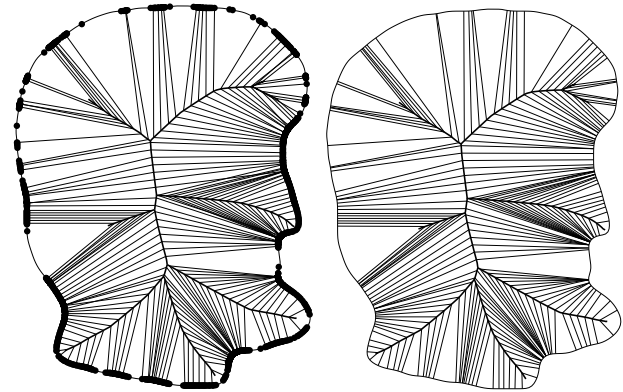


**Figure 7**. For each shape the original is shown in gray, the skeleton obtained using the average outward flux is shown with curves and the boundary points estimated from the skeleton using the relationship between the average outward flux and the object angle $\alpha$ are shown with black circles.



**Figure 8**. Bi-tangent points associated with regular skeletal points: (LEFT) computed using average outward flux information and (RIGHT) computed explicitly.

ing skeletal points. In particular, we have shown that the average outward flux through a shrinking region containing a skeletal point tends to a nonzero value, whereas it vanishes for non-skeletal points. An analysis assuming shrinking circular regions shows that the average outward flux also reveals the object angle for the three types of skeletal points, allowing for the boundary to be explicitly reconstructed given a parametrization of the skeleton. Thus the average outward flux measure can be viewed as a Euclidean invariant for shape description: it can be used to both detect the skeleton as well as to explicitly reconstruct the boundary from it. We have presented several numerical experiments to corroborate the theory.

## References

[1] A. J. Chorin and J. E. Marden. *A Mathematical Introduction to Fluid Mechanics*. Springer-Verlag, 1993.

[2] J. N. Damon. Global geometry of regions and boundaries via skeletal and medial integrals. *manuscript in preparation*, 2003.

[3] P. Dimitrov, C. Phillips, and K. Siddiqi. Robust and efficient skeletal graphs. In *CVPR'00*, volume 1, pages 417–423, 2000.

[4] J. C. Lagarias, J. A. Reeds, M. H. Wright, and P. E. Wright. Convergence properties of the nelder-mead simplex algorithm in low dimensions. *SIAM Journal on Optimization*, 9:112–147, 1998.

[5] T. Sebastian, P. Kline, and B. B. Kimia. Recognition of shapes by editing shock graphs. In *International Conference on Computer Vision*, pages 755–761, Vancouver, Canada, July 2001.

[6] K. Siddiqi, S. Bouix, A. Tannenbaum, and S. W. Zucker. The hamilton-jacobi skeleton. In *International Conference on Computer Vision*, pages 828–834, Kerkyra, Greece, September 1999.

[7] K. Siddiqi, S. Bouix, A. Tannenbaum, and S. W. Zucker. Hamilton-jacobi skeletons. *International Journal of Computer Vision*, 48(3):215–231, 2002.

[8] K. Siddiqi, A. Shokoufandeh, S. J. Dickinson, and S. W. Zucker. Shock graphs and shape matching. *International Journal of Computer Vision*, 35(1):13–32, 1999.

[9] G. D. Stetten and S. M. Pizer. Automated identification and measurement of objects via populations of medial primitives, with application to real time 3d echocardiography. In *International Conference on Information Processing in Medical Imaging*, pages 84–97, 1999.

[10] A. Torsello and E. R. Hancock. A skeletal measure of 2d shape similarity. In *Proceedings of the International Workshop On Visual Form*, volume LNCS 2059, pages 260–271, 2001.